Self-healing catalysis in water

Cyrille Costentin[a,1] and Daniel G. Nocera[b,1]

[a]Laboratoire d'Electrochimie Moléculaire, Unité Mixte de Recherche Université–CNRS 7591, Université Paris Diderot, Sorbonne Paris Cité, 75205 Paris Cedex 13, France; and [b]Department of Chemistry and Chemical Biology, Harvard University, Cambridge, MA 02138

Edited by Michael L. Klein, Temple University, Philadelphia, PA, and approved August 11, 2017 (received for review July 1, 2017)

Principles for designing self-healing water-splitting catalysts are presented together with a formal kinetics model to account for the key chemical steps needed for self-healing. Self-healing may be realized if the catalysts are able to self-assemble at applied potentials less than that needed for catalyst turnover. Solution pH provides a convenient handle for controlling the potential of these two processes, as demonstrated for the cobalt phosphate (CoP_i) water-splitting catalyst. For Co^{2+} ion that appears in solution due to leaching from the catalyst during turnover, a quantitative description for the kinetics of the redeposition of the ion during the self-healing process has been derived. The model reveals that OER activity of CoP_i occurs with negligible film dissolution in neutral pH for typical cell geometries and buffer concentrations.

solar energy | water splitting | renewable energy storage | self-healing catalysis | cobalt phosphate

Water is a desirable medium for storing solar energy. Charge-separated states generated by solar capture in semiconductors may be transferred directly or indirectly to catalysts, which rearrange the chemical bonds of water to produce the high-energy products of oxygen and hydrogen (1, 2). Hydrogen may be used directly as a fuel (3, 4) or converted into a liquid fuel with its combination with carbon dioxide via inorganic (5) or hybrid biological–inorganic catalysts (6–8). In addition, renewable hydrogen may be used to derive other energy-intensive products (9) such as ammonia for fertilization (10). Although an atomically simple conversion, the bond rearrangement of two water molecules to hydrogen and oxygen is chemically complex. The reaction encompasses a four-electron process, and this multielectron inventory must be coupled intimately to protons (11) to avoid the high-energy intermediates summarized on the Frost diagram of water (Fig. 1). Most water-splitting catalysis is performed in concentrated base (12). However, in contradistinction to the harsh conditions of basic water, the ease and simplicity of interfacing catalysts to semiconducting materials in fabricated devices such as buried junctions [e.g., the artificial leaf (13, 14)] is facilitated when neutral or near-neutral water is used, which also engenders greater materials stability and lessened liability for the implementation of new technologies. For these reasons, earth-abundant materials for water splitting at neutral and near-neutral conditions is now generally being adopted as a preferred approach for achieving direct photoelectrochemical energy conversion processes (15). Nonetheless, the use of pure water is insufficient to meet future global energy needs. Growth in energy during this century is projected to be driven by the urgent needs of emerging and low-income countries that currently lack access to reliable energy (16). Achieving the decarbonization needed to address climate change in the developing world has provided an imperative for the development of a distributed renewable energy infrastructure with minimal engineering requirements (17). Thus, solar driven water splitting should not be confined to pure water but be achieved with any local water source. These considerations have spurred us to design self-healing water splitting catalysts created from the earth-abundant elements of Mn, Co, and Ni (18–20). These catalysts continually renew themselves during catalyst operation, thus allowing natural water to be used for water splitting. This article will present the general design principles and accompanying formal kinetics analysis for performing self-healing, water-splitting catalysis.

Self-Healing by a Cobalt Phosphate OER Catalyst

A metric for catalysis performance is turnover number, which is described by Fig. 2, *Left*. Catalysis occurs from an active catalyst state, which is generated from a precatalytic resting state. During turnover between the catalyst and precatalyst (turnover being the number of times cycled between the two), the catalyst degenerates to an inactive form, which then must be regenerated to the pre-activated state, usually by a chemical process. The most active water-splitting catalysts are oxides, and the catalyst degenerative process usually involves dissolution, more commonly described as corrosion. In the oxygen evolution reaction (OER), the four-electron oxidation of water to oxygen is accompanied by the release of four protons. In basic solution, the strongest base at appreciable concentration is hydroxide OH^-, which neutralizes the released protons. However, in water at pH 7 or near-neutral conditions, the concentration of OH^- is only 10^{-5} to 10^{-9} M; the strongest base in water is therefore the oxide itself. As metal oxides are basic in the Lux classification of bases (21), they readily react with acid. Excluding critical noble elements (e.g., Ru and Ir), reaction of acid with the oxides of earth-abundant metals (e.g., first row transition metals) thus leads to corrosion by the leaching of metal ions and dissolution of the oxide. To overcome corrosion in water, the self-healing Co, Mn, and Ni catalysts balance their self-assembly in the presence of phosphate (P_i) or borate (B_i) anions with OER catalysis such that the equilibrium for self-assembly (i.e., catalyst regeneration) lies energetically within that for OER catalysis (Fig. 2, *Right*). The self-healing catalyst is distinguished by turnover number that is infinite; that is, as long as the catalyst is operating, it is able to heal itself.

The active sites of the exemplar CoP_i catalyst are cobaltate clusters (22–25). Isotopic oxygen labeling studies have shown that OER occurs at edge sites of the cobaltate clusters, with a dicobalt active site as the minimal structural unit that supports catalysis (Fig. 3) (26). OER catalysis proceeds from a Co(III) "Co(IV)" precatalyst (**P**) state, as shown by X-ray absorption spectroscopy (XAS) (22, 27) and

Significance

Water provides an attractive medium for storing solar energy via water splitting. Charge-separated states generated by solar capture may be transferred to catalysts that split water to hydrogen and oxygen. Most water-splitting catalysts comprising earth-abundant elements are susceptible to corrosion when operated in neutral and natural water. Such corrosion may be circumvented if the catalysts are self-healing. The design of self-healing catalysts allows neutral water and natural water sources to be used for water splitting, greatly simplifying the implementation of using water as a distributed energy storage medium for solar energy.

Author contributions: C.C. and D.G.N. designed research, performed research, contributed new reagents/analytic tools, analyzed data, and wrote the paper.

The authors declare no conflict of interest.

This article is a PNAS Direct Submission.

[1]To whom correspondence may be addressed. Email: dnocera@fas.harvard.edu or cyrille.costentin@univ-paris-diderot.fr.

This article contains supporting information online at www.pnas.org/lookup/suppl/doi:10.1073/pnas.1711836114/-/DCSupplemental.

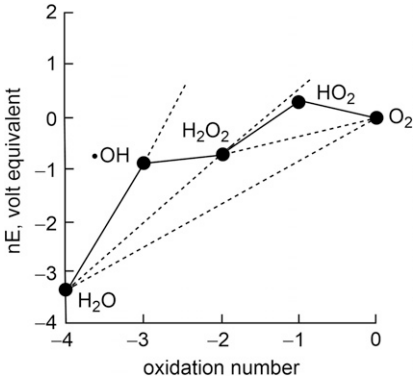

Fig. 1. Frost diagram for H_2O at pH 7. The apparent standard potential for redox couple is given by the slope of the line connecting the two species on a Frost diagram.

Electron Paramagnetic Resonance (EPR) Spectroscopy (28). Localized at the edges of the cobaltate clusters, the "Co(IV)" centers may be reformulated as a Co(III)–O• oxyl radical as a direct consequence of the electronic considerations embodied by the "oxo wall" (29). Tafel analysis of the CoP_i catalysis acquired over a range of conditions (pH, $[Co^{2+}]$, and $[P_i]$) furnishes the rate law for OER (25) to be

$$j = 4F\Gamma_{CoP_i}k_0^{OER}\frac{1}{[H^+]}\exp\left[\frac{FE}{RT}\right], \quad [1]$$

where j is the current density, F is Faraday's constant, Γ_{CoP_i} is the surface concentration of CoP_i deposited onto the electrode, and k_0^{OER} is a potential-independent constant that is proportional to the exchange current density. The rate law therefore reveals a $1e^-|1H^+$ PCET minor equilibrium to generate the active "Co(IV) Co(IV)" catalyst (**C**) (25), which drives O–O bond formation and the release of O_2 in a turnover rate-limiting chemical step.

Self-healing in CoP_i is established from the interplay of the potential at which OER occurs vs. the potential at which the catalyst self-assembles. The CoP_i catalyst self-assembles from phosphate solution containing Co^{2+} ions upon the application of applied potentials 0.2 V negative of the potential needed for water splitting (18, 25). At these potentials, Co^{2+} is oxidized to Co^{3+}, which is substitutionally inert, resulting in initial deposition of the film. Electrochemical kinetics data were obtained for catalyst growth as a function of Co^{2+} concentration, pH, and P_i concentration (30). Tafel plots revealed a catalyst assembly mechanism involving a one-electron reversible equilibrium preceding a chemical rate-limiting step to catalyst formation. A first-order dependence on Co^{2+} concentration established that this reversible one-electron equilibrium involved Co^{2+} ion in solution. Additionally, the rate of deposition possessed an inverse third-order dependence on proton activity and an inverse dependence on P_i, giving an electrochemical rate law for catalyst formation and growth as

$$j = Fk_0^{sa}\frac{[Co^{2+}]}{[H^+]^3[P_i]}\exp\left[\frac{FE}{RT}\right], \quad [2]$$

where k_0^{sa} is a potential-independent constant that is proportional to the exchange current density for the electrodeposition self-assembly process. A model (Fig. 4) consistent with this rate law has been constructed from studies of CoP_i and molecular cobaltate cluster model complexes. At the deposition potential, a small amount of Co^{4+} is present in the film, as is consistent with the Nernst equation and verified by EPR spectra of CoP_i films (28). The transport of the Co^{4+} in CoP_i films (i.e., the oxidizing hole equivalent) is predicted to be fast based on the $Co^{3+/4+}$ self-exchange electron transfer rate constant of $k_{ET}(Co^{3+/4+}) = 3 \times 10^5\ M^{-1}\cdot s^{-1}$ measured in cobalt cubane model complexes (31). Delivery of the hole equivalent to the surface of the catalyst allows Co^{4+} in CoP_i to react with Co^{2+} in solution to yield Co^{3+}, which adds to edges exposed from dissociation of P_i from the cobalt cluster, as observed in substitution kinetics studies of native CoP_i (26) and Co_7 metallate clusters (32). These results account for the first order in $[Co^{2+}]$ and inverse order in $[P_i]$. Important to the self-healing process, the rate of deposition possesses an inverse third-order dependence on proton activity arising for the need of $Co(H_2O)_6^{2+}$ to be deprotonated so that the ion can be oxidized at potentials of ~1.0 V (33). The remaining proton inventory results from a proton accompanying the dissociation of P_i at pH 7, and the oxidation of Co^{3+} to Co^{4+} occurs by a $1e^-|1H^+$ PCET, as observed for the oxidation of a Co^{3+} center to Co^{4+} in cobalt cubane complexes (31).

The mechanistic basis for CoP_i self-healing is rooted in Eqs. **1** and **2**. Because $\log(j)$ scales with E, the Pourbaix diagram for OER and catalyst self-assembly may be constructed from the $\partial E/\partial pH$ dependence for the two processes (25, 30) as described by Eqs. **1** and **2**. The determinant factor for self-healing in CoP_i is that the electrodeposition process displays an inverse third-order dependence on proton activity, whereas OER displays a first-order dependence on proton activity. The potential necessary for catalyst self-assembly therefore rises much more rapidly with decreasing pH compared with that for OER. In the green-highlighted zone of Fig. 5, the potentials necessary to sustain catalyst film nucleation and growth are well below the potentials required for OER catalysis. Thus, as long as the catalyst is operated in the green zone, the CoP_i is indefinitely stable in water. Indeed, we have shown by ^{57}Co radiolabeling of CoP_i films (34) that no cobalt ions are observed in solution when the catalyst is operated at potentials within Fig. 5's green zone of stability. We note that the CoP_i self-assembly data in Fig. 5 were measured over the HPO_4^{2-} buffering pH range of 7–9; extrapolation of the curve predicts catalyst corrosion at pH < 5.2. The validity of the extrapolation is confirmed by measurements of the fraction of catalyst film dissolved, as deduced by elemental analysis and solubilized Co^{2+} and Co^{2+}-induced paramagnetic line broadening of the ^{31}P NMR peak of the phosphate electrolyte; the CoP_i catalyst is observed to corrode only when the pH is less than 5.5 (30). Controlling the interplay in $\partial E/\partial pH$ for OER and self-assembly can lead to extraordinary properties of catalysts; for instance, an oxidic Mn catalyst self-assembles via a disproportionation reaction of two Mn^{3+} ions that is fourth-order in proton concentration (35), allowing catalyst stability via self-healing to be achieved at pHs as low as –0.5.

A Formal Kinetics Model for Self-Healing

Each turnover of OER drops the catalyst to a formal redox level of Co^{2+}. If the self-exchange electron transfer by hole hopping

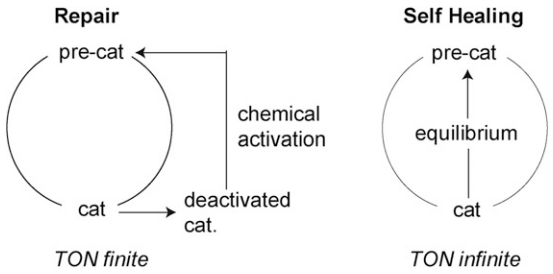

Fig. 2. A catalyst that is repaired versus self-healing.

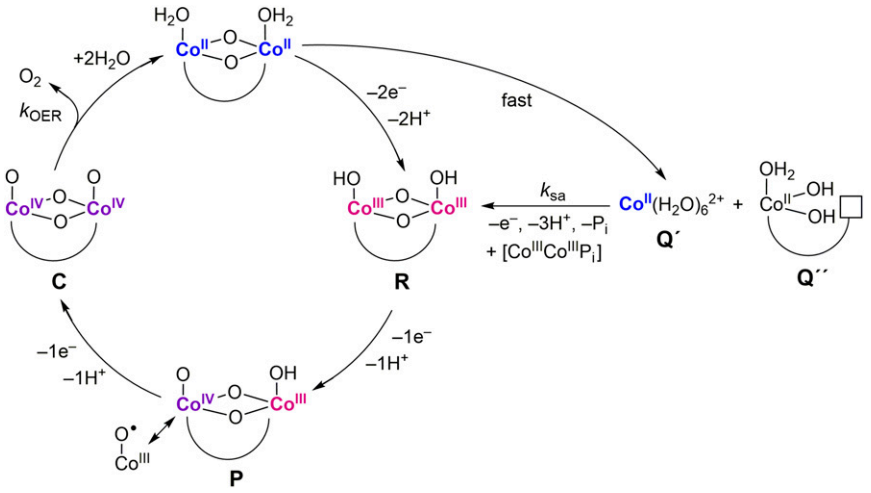

Fig. 3. OER pathway for CoP_i as determined from electrochemical kinetics, EPR, and XAS studies. Curved lines connecting Co metal centers denote phosphate or OH_x terminal or bridging ligands. The path on the far right is the self-assembly pathway to reconstitute the catalyst. Fig. 4 delineates the pathway in greater detail. The alphabetical labels used for developing the kinetics expressions derived in *SI Appendix*. The [$Co^{III}Co^{III}P_i$] species represents Co^{III} edge sites, which at the edge can hydrogen bond to P_i in solution (lower left species in Fig. 4, vide infra).

through the film is fast enough to furnish Co^{3+}, then the catalyst does not access the self-healing cycle on the right side of Fig. 4. Those Co^{2+} ions (**Q′**) that are released into solution are reincorporated into the CoP_i catalyst by the self-assembly process shown in Fig. 4 and characterized by an overall apparent rate constant, k_{sa}. Owing to the fast $Co^{3+/4+}$ self-exchange electron transfer in the CoP_i film, the oxidation of the Co^{2+} ions by Co^{4+} in the film may be considered as an oxidation promoted at the electrode. The rate constant for self-assembly in the absence of buffer mass transport limitation is

$$k_{sa}(E) = k^0_{sa}\frac{(C_0)^4}{[H^+]^3[P_i]}\exp\left[\frac{FE}{RT}\right], \qquad [3]$$

where C_0 is a normalization concentration and k^0_{sa} is the intrinsic rate constant. Similarly, the rate constant for OER catalysis is

$$k_{OER}(E) = k^0_{OER}\frac{C_0}{[H^+]}\exp\left[\frac{FE}{RT}\right], \qquad [4]$$

where k^0_{OER} is the intrinsic catalytic rate constant. Note that the C_0 normalization concentration delivers intrinsic rate constants k^0_{sa} and k^0_{OER} in the same units as $k_{sa}(E)$ and $k_{OER}(E)$, i.e., $cm{\cdot}s^{-1}$ and s^{-1}, respectively, so that their ratio is an intrinsic distance to be compared with a characteristic geometrical distance of the electrochemical cell (vide infra). When $C_0 = 1$ M, Eqs. **3** and **4** reduce to Eqs. **2** and **1**, respectively. As the catalytic reaction is operated in absence of Co^{2+} is solution, the driving force for mass transport to release Co^{2+} ions into bulk solution can attenuate the self-assembly process (noting that even though the entire catalyst can dissolve at open circuit potential over days, it immediately reforms upon the application of an applied potential for OER).

A formal kinetics analysis of the self-healing process reduces to a treatment of the concentration of released Co^{2+} ion into solution. The CoP_i catalyst is considered to operate at a constant electrode potential E in a solution containing a large concentration of buffer and under well-defined hydrodynamic (i.e., a constant diffusion layer) and linear diffusion conditions (*SI Appendix*). Under these boundary conditions, Co^{2+} ion will accumulate in the bulk solution during a transient period characterized by a time constant τ,

$$\tau = \frac{1+\frac{k_{sa}(E)}{D/\delta}}{k_{OER}(E)+\frac{k_{sa}(E)}{V/S}}, \qquad [5]$$

where V is the volume of the solution, S is the electrode surface area, D is $Co(H_2O)_6^{2+}$ diffusion coefficient, and δ is the size of

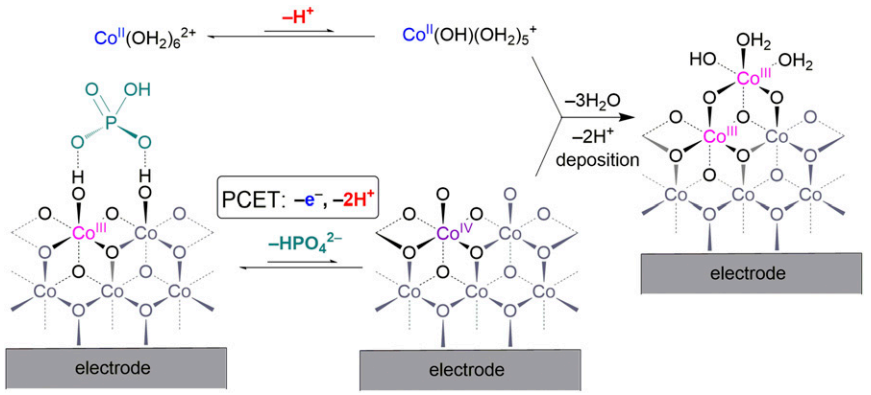

Fig. 4. Proposed mechanism of CoP_i catalyst self-assembly.

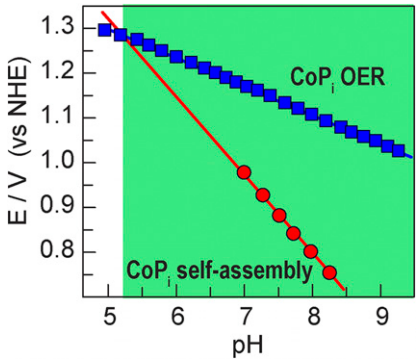

Fig. 5. Pourbaix diagram for CoP_i OER (blue squares) and self-assembly (red circles) at $j = 30\ \mu A \cdot cm^{-2}$. Data from ref. 30.

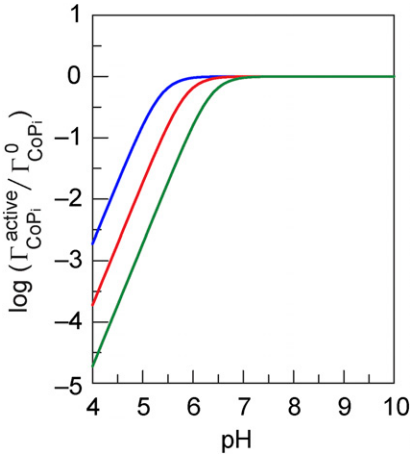

Fig. 6. Evolution of the fraction of steady-state active form of CoP_i catalyst as function of pH according to Eq. **6** with $k^0_{sa} = 2.63 \times 10^{-43}\ cm \cdot s^{-1}$ and $k^0_{OER} = 1.39 \times 10^{-30}\ s^{-1}$ (see text), $V/S = 1$ cm and $[P_i] = 0.01$ M (blue line—), $V/S = 10$ cm and $[P_i] = 0.01$ M (red line), and $V/S = 10$ cm and $[P_i] = 0.1$ M (green line).

the diffusion layer. A steady-state situation is attained when $t >> \tau$, in which the fraction of remaining active film after equilibration with the bulk solution at a given pH can be written (*SI Appendix*) as

$$\frac{\Gamma^{active}_{CoP_i}}{\Gamma^{0}_{CoP_i}} = \frac{\frac{k^0_{sa}}{\frac{V}{S}k^0_{OER}}}{\frac{[H^+]^2[P_i]}{(C^0)^3} + \frac{k^0_{sa}}{\frac{V}{S}k^0_{OER}}}. \quad [6]$$

The fraction in Eq. **6** depends on a geometrical parameter V/S (the electrochemical cell depth) as well as on intrinsic properties of the catalyst, k^0_{sa}/k^0_{OER}. Due to the Nernstian behavior of all electron transfer reactions, the fraction in Eq. **6** is independent of potential but, importantly, depends on the self-assembly elements of pH and buffer concentration [the CoP_i films are considered in a catalytic regime where neither buffer transport outside the film or PCET transport within the film, as previously described (36), interfere].

From experimental data indicating that the catalytic OER current density for a 24 $mC \cdot cm^{-2}$ deposited film is $j = 30\ \mu A \cdot cm^{-2}$ at pH 7 and $E = 1.16$ V vs. normal hydrogen electrode (NHS) (25), we evaluate $k^0_{OER} = 1.39 \times 10^{-30}\ s^{-1}$. Similarly, from experimental data noting that a deposition current density of $j = 30\ \mu A \cdot cm^{-2}$ is attained at 0.975 V vs. NHE from a 0.02 M pH 7 buffer and 0.4 mM Co^{2+} solution of ref. 30, we evaluate $k^0_{sa} = 2.63 \times 10^{-43}\ cm \cdot s^{-1}$. Fig. 6 shows that the critical pH that defines the zone of self-healing depends on the cell geometry (V/S) and buffer concentration ($[P_i]$). The onset of the zone occurs at a pH consistent with the experimental observation of Fig. 5.

Conclusion

Self-healing can be imbued on a heterogeneous or molecular catalyst if it can self-assemble at applied potentials less than that needed for catalyst operation. Solution pH provides a convenient handle for controlling potential, which may be adjusted with greater fidelity for self-assembly if the proton dependence occurs at greater order than that for catalysis. For CoP_i, the proton dependence is third order versus a first-order dependence for OER; accordingly, $\partial E/\partial pH$ in the Pourbaix diagram for self-assembly shows a much steeper slope than OER enabling the conditions for self-healing to be achieved over a wide pH range that includes neutral water. For Co^{2+} ion that appears in solution, a quantitative description for the kinetics of the redeposition of the ion has been derived. These results show that OER activity of CoP_i occurs with negligible film dissolution in neutral pH for typical cell geometries and buffer concentrations. Such design of self-healing catalysts allows neutral water and natural water sources to be used for water splitting, greatly simplifying the implementation of using water as a distributed energy storage medium for solar energy.

ACKNOWLEDGMENTS. We thank Evan Jones for helpful discussions. This material is based upon work supported with Grant DE-SC0017619 from the Solar Photochemistry Program of the Chemical Sciences, Geosciences and Biosciences Division, Office of Basic Energy Sciences of the US Department of Energy.

1. Lewis NS, Nocera DG (2006) Powering the planet: Chemical challenges in solar energy utilization. *Proc Natl Acad Sci USA* 103:15729–15735.
2. Lewis NS, Nocera DG (2015) The solar opportunity. *The Bridge* 46:41–47.
3. Turner JA (2004) Sustainable hydrogen production. *Science* 305:972–974.
4. Cook TR, et al. (2010) Solar energy supply and storage for the legacy and nonlegacy worlds. *Chem Rev* 110:6474–6502.
5. Li CW, Ciston J, Kanan MW (2014) Electroreduction of carbon monoxide to liquid fuel on oxide-derived nanocrystalline copper. *Nature* 508:504–507.
6. Torella JP, et al. (2015) Efficient solar-to-fuels production from a hybrid microbial-water-splitting catalyst system. *Proc Natl Acad Sci USA* 112:2337–2342.
7. Liu C, Colón BC, Ziesack M, Silver PA, Nocera DG (2016) Water splitting-biosynthetic system with CO_2 reduction efficiencies exceeding photosynthesis. *Science* 352:1210–1213.
8. Nichols EM, et al. (2015) Hybrid bioinorganic approach to solar-to-chemical conversion. *Proc Natl Acad Sci USA* 112:11461–11466.
9. Nocera DG (2017) Solar fuels and solar chemicals industry. *Acc Chem Res* 50:616–619.
10. Liu C, Sakimoto KK, Colón BC, Silver PA, Nocera DG (2017) Ambient nitrogen reduction cycle using a hybrid inorganic-biological system. *Proc Natl Acad Sci USA* 114:6450–6455.
11. Cukier RI, Nocera DG (1998) Proton-coupled electron transfer. *Annu Rev Phys Chem* 49:337–369.
12. Surendranath Y, Nocera DG (2011) Oxygen evolution reaction chemistry of oxide–based electrodes. *Prog Inorg Chem* 57:505–560.
13. Reece SY, et al. (2011) Wireless solar water splitting using silicon-based semiconductors and earth-abundant catalysts. *Science* 334:645–648.
14. Nocera DG (2012) The artificial leaf. *Acc Chem Res* 45:767–776.
15. Sun K, et al. (2016) A stabilized, intrinsically safe, 10% efficient, solar-driven water-splitting cell incorporating earth-abundant electrocatalysts with steady-state pH gradients and product separation enabled by a bipolar membrane. *Adv Energy Mater* 6:1600379.
16. Nocera DG (2006) On the future of global energy. *Daedalus* 135:112–115.
17. Nocera DG (2012) Can we progress from solipsistic science to frugal innovation? *Daedalus* 141:45–52.
18. Kanan MW, Nocera DG (2008) In situ formation of an oxygen-evolving catalyst in neutral water containing phosphate and Co^{2+}. *Science* 321:1072–1075.
19. Bediako DK, et al. (2012) Structure-activity correlations in a nickel-borate oxygen evolution catalyst. *J Am Chem Soc* 134:6801–6809.
20. Huynh M, Bediako DK, Nocera DG (2014) A functionally stable manganese oxide oxygen evolution catalyst in acid. *J Am Chem Soc* 136:6002–6010.
21. Lux H (1939) "Säuren" und "basen" im schmelzfluss: Die bestimmung der sauerstoffionenkonzentration. *Ztschr Elektrochem* 45:303–309.
22. Kanan MW, et al. (2010) Structure and valency of a cobalt-phosphate water oxidation catalyst determined by in situ X-ray spectroscopy. *J Am Chem Soc* 132:13692–13701.
23. Farrow CL, Bediako DK, Surendranath Y, Nocera DG, Billinge SJL (2013) Intermediate-range structure of self-assembled cobalt-based oxygen-evolving catalyst. *J Am Chem Soc* 135:6403–6406.
24. Du P, Kokhan O, Chapman KW, Chupas PJ, Tiede DM (2012) Elucidating the domain structure of the cobalt oxide water splitting catalyst by X-ray pair distribution function analysis. *J Am Chem Soc* 134:11096–11099.

25. Surendranath Y, Kanan MW, Nocera DG (2010) Mechanistic studies of the oxygen evolution reaction by a cobalt-phosphate catalyst at neutral pH. *J Am Chem Soc* 132: 16501–16509.
26. Ullman AM, Brodsky CN, Li N, Zheng SL, Nocera DG (2016) Probing edge site reactivity of oxidic cobalt water oxidation catalysts. *J Am Chem Soc* 138:4229–4236.
27. Brodsky CN, et al. (2017) In situ characterization of cofacial Co(IV) centers in Co4O4 cubane: Modeling the high-valent active site in oxygen-evolving catalysts. *Proc Natl Acad Sci USA* 114:3855–3860.
28. McAlpin JG, et al. (2010) EPR evidence for Co(IV) species produced during water oxidation at neutral pH. *J Am Chem Soc* 132:6882–6883.
29. Winkler JR, Gray HB (2012) Electronic structures of oxo-metal ions. *Structure and Bonding*, eds Mingos DMP, Day P, Dahl JP (Springer, Berlin), Vol 142, pp 17–28.
30. Surendranath Y, Lutterman DA, Liu Y, Nocera DG (2012) Nucleation, growth, and repair of a cobalt-based oxygen evolving catalyst. *J Am Chem Soc* 134:6326–6336.
31. Symes MD, Surendranath Y, Lutterman DA, Nocera DG (2011) Bidirectional and unidirectional PCET in a molecular model of a cobalt-based oxygen-evolving catalyst. *J Am Chem Soc* 133:5174–5177.
32. Ullman AM, Nocera DG (2013) Mechanism of cobalt self-exchange electron transfer. *J Am Chem Soc* 135:15053–15061.
33. Sisley MJ, Jordan RB (2006) First hydrolysis constants of hexaaquacobalt(III) and -manganese(III): Longstanding issues resolved. *Inorg Chem* 45:10758–10763.
34. Lutterman DA, Surendranath Y, Nocera DG (2009) A self-healing oxygen-evolving catalyst. *J Am Chem Soc* 131:3838–3839.
35. Huynh MD, Bediako DB, Liu Y, Nocera DG (2014) Nucleation and growth mechanisms of an electrodeposited manganese oxide oxygen evolution catalyst. *J Phys Chem C* 118:17142–17152.
36. Bediako DK, Costentin C, Jones EC, Nocera DG, Savéant JM (2013) Proton-electron transport and transfer in electrocatalytic films. Application to a cobalt-based O_2-evolution catalyst. *J Am Chem Soc* 135:10492–10502.